


NANO IDEA

Open Access



A Facile Method for Preparation of Cu₂O-TiO₂ NTA Heterojunction with Visible-Photocatalytic Activity

Yulong Liao^{1,2*} , Peng Deng¹, Xiaoyi Wang¹, Dainan Zhang¹, Faming Li², Qinghui Yang¹, Huaiwu Zhang¹ and Zhiyong Zhong¹

Abstract

Based on highly ordered TiO₂ nanotube arrays (NTAs), we successfully fabricated the Cu₂O-TiO₂ NTA heterojunction by a simple thermal decomposition process for the first time. The anodic TiO₂ NTAs were functioned as both “nano-container” and “nano-reactors” to load and synthesize the narrow band Cu₂O nanoparticles. The loaded Cu₂O expanded absorption spectrum of the TiO₂ NTAs from ultraviolet range to visible light range. We found that the Cu₂O-TiO₂ NTA heterojunction films had visible activity towards photocatalytic degrading methyl orange (MO). The photocatalytic abilities of the Cu₂O-TiO₂ NTA heterojunction films were found increased with the Cu₂O content from 0.05 to 0.3 mol/L. This could be explained by more electron-hole pairs generated and less recombination, when the Cu₂O-TiO₂ heterojunction got formed. Here, we put forward this promising method, hoping it can facilitate the mass production and applications of Cu₂O-TiO₂ NTA heterojunction.

Keywords: TiO₂ nanotube, Cu₂O, Heterojunction, Thermal decomposition, Visible photocatalysis

Background

With more and more attention paid to the environmental issues nowadays, the study of water treatment materials emerged in a continuous stream [1–4]. Hundreds of strategies were proposed for the treatment of polluted water. However, there were many problems, such as low efficiency, low recycling rate, and secondary environment pollution, restricting their further applications [5–7]. The semiconductor materials were considered to be a promising candidate, and titanium oxide was recognized as one of the best photocatalyst materials due to its high photocatalytic activity and good chemical and mechanical stability [8–12]. Recently, TiO₂ materials with nanotube (NT) array were widely studied, and the tubular morphology was proved to be a promising structure for photocatalysis. Compared with other microcosmic morphologies, TiO₂ NT arrays owned

several significant advantages [13–17]. Firstly, unique tubular structure could enhance electron-transporting efficiency and restrain the recombination of carriers, which will further produce more reactive oxygen species (ROS) [18, 19]. Secondly, TiO₂ NT arrays are much easier to recycle than the TiO₂ powder photocatalysts [20–24]. Thirdly, TiO₂ NT arrays have large specific surface area and high surface energy. However, due to the relatively wide gaps (~ 3.2 eV). TiO₂ NT photocatalyst is only active under UV irradiation [25–28]. In fact, a photocatalyst that is able to respond with visible light will surely take obvious advantages. At present, the focus of photocatalyst research is to adjust their light response band and improve their photocatalytic efficiency.

Building heterogeneous TiO₂ photocatalysts with narrow band gaps is one of the hotspots as an attempt to overcome such impediments. Narrow band semiconductors, like Cu₂O, CdS, CdTe, PbS, and Bi₂O₃, have been studied to build TiO₂ heterojunction photocatalysts [29–34]. Among them, Cu₂O (with the direct gap

* Correspondence: yulong.liao@uestc.edu.cn

¹State Key Laboratory of Electronic Thin Film and Integrated Devices, University of Electronic Science and Technology of China, Chengdu 610054, China

²Center for Applied Chemistry, University of Electronic Science and Technology of China, Chengdu 611731, China

of ~ 2.2 eV) is regarded as one of the best candidates. For Cu_2O , the response band is about 560 nm, and its band gap structure happens to well match with the energy level of TiO_2 NTs. As schematically shown in Fig. 1, under the excitation of visible light, electron/hole pairs are generated and the photoinduced electrons are excited to the conduction band of Cu_2O and then transfer to the conduction band of TiO_2 , which suppresses the recombination of electrons and holes. This heterojunction structure solves the problem that the TiO_2 materials could not respond to visible light and the problem that electron/hole pairs generated on Cu_2O get recombined easily. From this point of view, Cu_2O - TiO_2 NTA heterojunction structure materials guaranteed a natural advantage in visible light photocatalysis.

General approach to prepare Cu_2O - TiO_2 heterojunction photocatalysts includes chemical coprecipitation and electrodeposition, and the products have shown promising photocatalytic performances. But it is still a challenge to prepare Cu_2O - TiO_2 heterojunction photocatalysts with good quality by using a facile and low-cost method. Inspired by the concept of the precursor from Chemical vapor deposition (CVD), the idea, using acetate to carry copper ion to get into the inside of TiO_2 NTs prepared by anodic oxidation, comes out. It is known that metal organic compounds are likely to get thermally decomposed. In this study, anodic TiO_2 NTAs were functioned as “nano-container” to load copper acetate at first and then as “nano-reactors” to provide space for thermal decomposing the loaded copper acetate. After a thermal treatment, Cu_2O - TiO_2 TNA heterojunction films were successfully obtained. To the best our knowledge, this method has not been reported to prepare Cu_2O - TiO_2 TNA heterojunction. Furthermore, the phase composition, morphology, and photocatalytic activity were characterized by XRD, EDS, SEM, and spectrophotometer.

Experimental Section

The chemicals which were mentioned in the experiment process were purchased (Sinopharm Group Chemical Reagent Co. Ltd., China) and used without further purification, except the deionized water with a resistance of $18.3 \text{ M}\Omega \text{ cm}$.

Preparation of Pure TiO_2 Nanotube Arrays

Anodic oxidation method was used to prepare uniform and stable TiO_2 NTAs with vertical alignment [35, 36]. Metal titanium (Ti) sheets were cut into pieces of $1.5 \times 5 \text{ cm}^2$ and cleaned by a cleanser. After a sonication bath in ethanol, the Ti pieces were dried in oven. Electrolyte consisted of 535.45 g glycol, 10 g deionized water, and 1.6617 g NH_4F , which were mixed and stirred for 2 h. Then, we took two pieces of Ti as anode and cathode, respectively. Immersing them into electrolyte, applying a constant potential of 50 V for 2 h, amorphous TiO_2 nanotube arrays (TiO_2 NTAs) were fabricated at room temperature.

Synthesis of Cu_2O - TiO_2 NTA Heterojunction

The amorphous TiO_2 NTAs were crystallized into anatase by a thermal treatment at 450°C . And then, they were used as substrate to prepare Cu_2O - TiO_2 NTA heterojunction film. First, cupric acetate ($\text{Cu}(\text{Ac})_2$) with different concentration was prepared, ranging from 0.05 to 0.3 mol/L. Then, annealed TiO_2 NTAs were immersed into the solution transiently and dried in oven at 70°C immediately. And the final products, Cu_2O - TiO_2 films, were marked as sample S1-S5 respectively by the different $\text{Cu}(\text{Ac})_2$ concentration of 0.05, 0.1, 0.2, 0.3, and 4 mol/L in this immersing process. After this process, the cupric acetate molecules had got into the TiO_2 nanotubes. Next step was putting the samples into an atmosphere-sintering furnace of N_2 with a sintering temperature of 400°C for 150 min. The cupric acetate

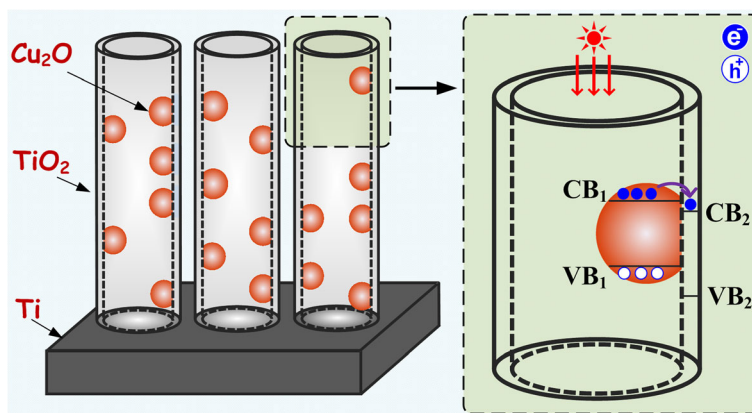
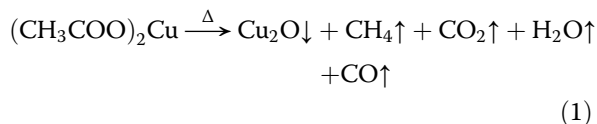


Fig. 1 Schematic structural diagram of Cu_2O - TiO_2 NTA heterojunction. Under visible light illumination, the electrons were excited to the conduction band of Cu_2O particles and then transferred to the conduction band of TiO_2 for the matching band gap structure

was thermal decomposed in a way described by Eq. (1). Finally, the $\text{Cu}_2\text{O-TiO}_2$ NTA heterojunction films were prepared. This process was schematically shown in Fig. 2.



Just like holding a test tube containing cupric acetate, after heating, cupric acetate thermal decomposed into Cu_2O which was left inside the TiO_2 NTAs.

Characterization

A scanning electron microscopy (SEM, JSM-7000F, JEOL Inc., Japan) with energy dispersive spectrometer (EDS) was used for the observation of the morphology and structure. The samples were characterized by a D/max-2400 X-ray diffraction spectrometer (Rigaku, D/max-2400, Japan) and a UV-vis spectrometry (Ultraspec 2100 pro) was also used. To evaluate the photocatalytic activity of the as-synthesized $\text{Cu}_2\text{O-TiO}_2$ NTA heterojunction, we took methyl orange (MO), a typical organic indicator, as the degraded object. The $\text{Cu}_2\text{O-TiO}_2$ NTA films ($3.0 \times 1.5 \text{ cm}^2$) were immersed in $5 \times 10^{-5} \text{ mol/L}$ of MO

aqueous solution and irradiated with seven 4 W visible bulbs (Toshiba, Cool white, FL4W, Japan). Then, the solution was magnetically stirred in the dark for 30 min to ensure adsorption-desorption equilibrium prior to photocatalytic degradation. Photodegradation experiments lasted 180 min with 1.5 mL samples withdrawn periodically. The concentration of the residual MO was measured by a spectrophotometer at about 460 nm on the basis of the Beer-Lambert law. The degradation efficiency of the MO could be defined as follows:

$$C_t/C_0 = (A_t/A_0) \times 100\% \quad (2)$$

And the varying of A_t/A_0 referred to the changing in C_t , which represented the photocatalytic activity of the tested samples.

Results and Discussion

Figure 3 shows a typical SEM observation of the pure anodic TiO_2 NTAs after annealing at $450 \text{ }^\circ\text{C}$. Anodizing is an electrolytic process which converts the outer surface of metals into an oxide layer or pore structure. As shown in Fig. 3, the as-prepared TiO_2 NTs have open-tube morphology with a uniform outer diameter distribution of $\sim 100 \text{ nm}$. The anodic TiO_2 NTAs are highly ordered and oriented, and each single TiO_2 NT owns very smooth tube walls with an average thickness of $\sim 10 \text{ nm}$. Our former

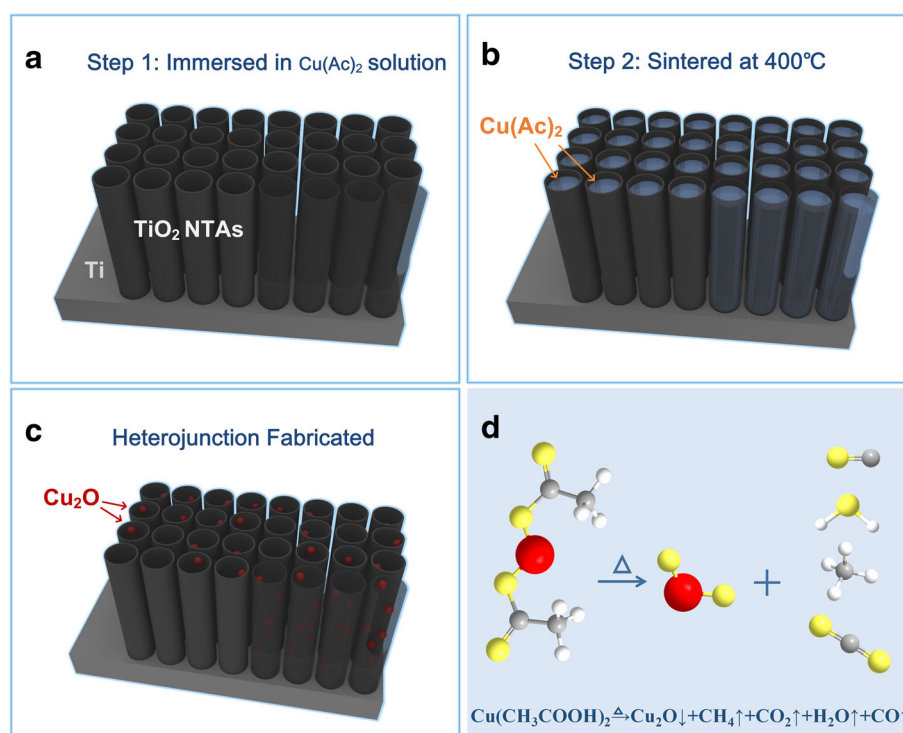


Fig. 2 Synthesis procedure of the $\text{Cu}_2\text{O-TiO}_2$ NTA heterojunction films. **a** Step 1, anodic TiO_2 NTAs. **b** Step 2, fill the tubes with precursor solution. **c** Step 3, sintered the filled tubes at $400 \text{ }^\circ\text{C}$ to get the $\text{Cu}_2\text{O-TiO}_2$ NTA heterojunction. **d** Chemical reaction formula of the sintering process

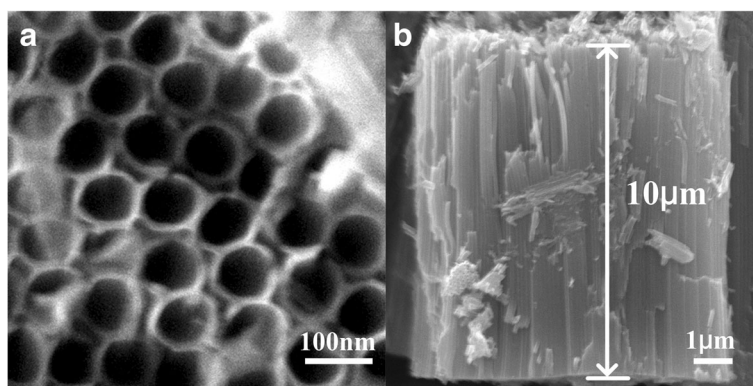


Fig. 3 Typical SEM images of pure TiO_2 nanotube arrays without modification. **a** Top view and **b** side view, indicating the highly ordered vertical alignment structure with open-tube mouth morphology. The tube diameter is about 100 nm, and the tube length is about 10 μm

studies have shown that tube length, the diameter, and morphology could be manipulated by adjusting the anodization protocols [37, 38]. The SEM results also indicate the thermal annealing at a high temperature of 450 °C does not destroy morphologies of the TiO_2 NTAs. XRD is used to characterize the crystalline of the pure TiO_2 NTAs (sample 1), see Fig. 4a. Results show that diffraction peaks locating at 25.3°, 36.9°, 37.8°, 48°, 53.9°, 55°, 62.7°, and 68.8° could be observed in sample 1, attributing to the (101), (103), (004), (200), (105), (211), (204), and (116) of anatase phase, respectively. As we know, there are three types of titanium dioxide phase, anatase, brookite, and rutile. Rutile could show relatively good photocatalytic ability with a granularity less than 10 nm. However, to get a rutile phase, the TiO_2 sample needs to be heated up to a high sinter temperature of 800 °C, which could lead to the break of TiO_2 tubes in this case. Brookite phase is hardly to be formed by using thermal annealing method for the bad thermodynamic phase stability, while anatase is the most common phase with good photocatalytic activity [39, 40]. The sharp diffraction peaks and the strong intensity of sample 1 (see Fig. 4a) indicated a highly

crystallized anatase structure, which meant our TiO_2 substrate was excellent not only in the morphology but also in the crystalline phase. The highly ordered TiO_2 NTAs with open-tube mouth morphology were used as substrate to prepare Cu_2O - TiO_2 NTA heterojunction films in this study.

XRD patterns of the TiO_2 NTAs loaded with Cu_2O nanoparticles in concentration gradient ranging from 0.05 to 4.0 mol/L are also shown in Fig. 4a, and the 4.0 mol/L sample was prepared by a cycling immerse process described in Additional file 1, the “Experimental Details” part. The samples were named samples 2 to 4 with the increasing $\text{Cu}(\text{Ac})_2$ concentration. Except the TiO_2 peaks, there was no peak of Cu_2O showing up in sample 2 because of the tiny amount of the loading Cu_2O particles. And particles might be decorated inside of the TiO_2 “nano-container” which also raised the difficulty for characterization. In sample 3 and sample 4, obvious cuprite peaks could be observed at 29.6°, 36.4°, 42.3°, and 61.3°, attributing to the cuprite (110), (111), (200), and (220) of Cu_2O , respectively. It should be noted here that sample 4 was only used to characterize

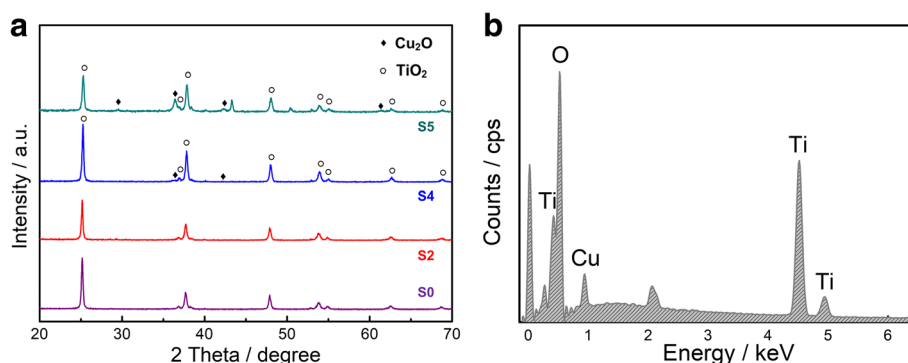


Fig. 4 a XRD patterns of the Cu_2O - TiO_2 NTA heterojunction samples. Sample S0: pure anatase TiO_2 NTA sample; samples S2, S4, and S5: thermally decomposed sample with immersing in 0.1, 0.3, and 4 mol/L $\text{Cu}(\text{Ac})_2$ solution, respectively. **b** EDS result of the Cu_2O - TiO_2 NTA heterojunction films, showing the existence of elements Ti, Cu, and O. The results confirm the successful loading of Cu_2O on the TiO_2 NTAs

the existence of Cu_2O particles, and its synthetic details were described in Additional file 1. Moreover, the lattice parameters and the grain size were calculated based on the XRD data. After removing the background and $K_{\alpha 2}$ diffraction, and following the smoothing and fitting process, we got the average lattice parameters of our samples of $a = b = c = 4.2646 \text{ \AA}$, which matched with the standard PDF. The standard PDF showed that the lattice parameters of Cu_2O are: $a = b = c = 4.2696 \text{ \AA}$, and Cu_2O had a cubic structure [41]. The average grain size of Cu_2O was calculated as $\sim 47 \text{ nm}$, by using Debye-Scherrer formula:

$$D = \frac{K\gamma}{B \cdot \cos\theta} \quad (3)$$

In Eq. (3), D is the grain size, K is the Scherrer constant, γ is the wavelength of X-ray, B is FWHM which needs to be in the radian, and θ is the diffraction angle. XRD results indicate that the $\text{Cu}(\text{Ac})_2$ were loaded into the TiO_2 NTAs and successfully decomposed into Cu_2O inside the same TiO_2 NTAs, and then the Cu_2O - TiO_2 NTA heterojunction films got formed. To further investigate the Cu_2O - TiO_2 NTA heterojunction, an elemental analysis was carried out by using EDS. Figure 4b showed an EDS diagram of Cu_2O - TiO_2 NTA heterojunction film which was prepared with 0.2 mol/L $\text{Cu}(\text{Ac})_2$. The atomic percentages were 7.32, 28.96, 57.45, and 6.27% for elements Cu, Ti, O, and impurity C. This result showed that the Cu_2O owned a relatively low content in the heterojunction sample, but it still brought about the visible-light activity, which would be discussed later in the MO degradation experiment. The EDS results well agreed with the XRD results in Fig. 4a that cuprite Cu_2O was successfully loaded to anatase NTAs.

Figure 5 showed the top view SEM results of the modified TiO_2 NTAs. Compared with the pure TiO_2 NTA samples in Fig. 3, a few small particles could be seen near the upper and inside of the TiO_2 tubes in Fig. 5a. Increasing the modification amount, a number of nanoparticles could be observed obviously in Fig. 5b.

Figure 5c was sample 4 that we discussed before. Large parts of the tube surface were covered by the redundant Cu_2O , indicating that sample 4 was over-decorated. Based on the SEM images, the size distribution of Cu_2O particles was estimated ranging from ~ 30 to $\sim 80 \text{ nm}$, which well agreed with XRD calculated grain size of $\sim 47 \text{ nm}$. For the tubular structure of the three samples, they still retained the vertical alignment state, but some tubes got a little awry. It was considered as the influence of thermal decomposition process, which needed a heating process of $400 \text{ }^\circ\text{C}$ to get $\text{Cu}(\text{Ac})_2$ decomposed into Cu_2O . High temperature in the decomposition step had a negative effect on the tubular structure, supported by the SEM images. However, if the heating temperature in the thermal process went too low to $240 \text{ }^\circ\text{C}$, $\text{Cu}(\text{CH}_3\text{COO})_2 \cdot \text{H}_2\text{O}$ would just get dehydrated instead of decomposed. So the temperature should be controlled in ~ 300 to $400 \text{ }^\circ\text{C}$ to keep the nano-scale tubular structure and ensure the fabrication of Cu_2O - TiO_2 NTA heterojunction. It can be concluded that the Cu_2O - TiO_2 heterojunction could be formed, and the morphology retained well, when the decomposition happens at $400 \text{ }^\circ\text{C}$.

The Cu_2O nanoparticles were loaded on TiO_2 NTAs to fabricate the heterojunction, which was expected to enhance the photo-response ability in visible light range, so UV-vis characterization was adopted to investigate optical properties of the as-synthesized Cu_2O - TiO_2 NTAs. Figure 6a shows the UV-vis absorption spectra of the Cu_2O - TiO_2 NTA samples with Cu_2O -loaded magnitude increasing from none to 4.0 mol/L . It could be seen in Fig. 6a that the pure TiO_2 NTAs without loading Cu_2O only showed out a high absorption in the ultraviolet region ($< 380 \text{ nm}$), due to its intrinsic material properties. After loading the Cu_2O particles, the absorption range was expanded to $600\text{--}700 \text{ nm}$. And when the intensity is increasing with the raising of the Cu_2O modification magnitude, the absorption value of the Cu_2O - TiO_2 heterojunction films also got increased. Figure 6a indicated that TiO_2 NTAs were given the visible light response ability by

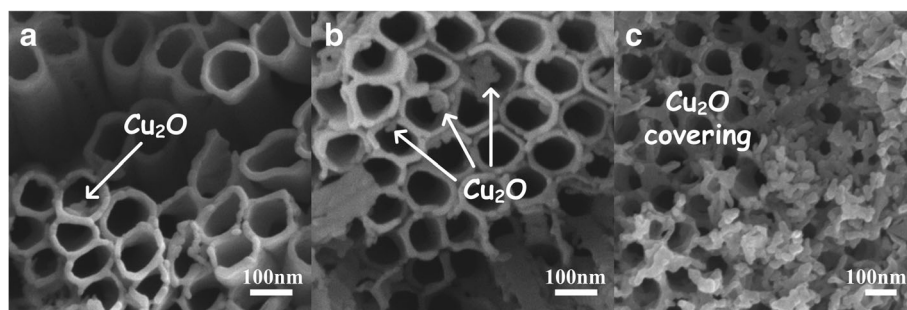


Fig. 5 Typical SEM images of the Cu_2O - TiO_2 NTA heterojunction films. **a** Sample immersed in 0.2 mol/L $\text{Cu}(\text{Ac})_2$. **b** Sample immersed in 0.3 mol/L $\text{Cu}(\text{Ac})_2$. **c** Sample immersed in $\text{Cu}(\text{Ac})_2$ of over high concentration

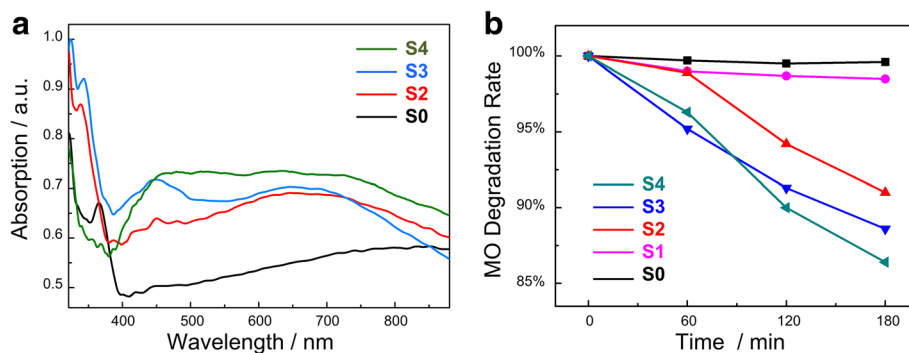


Fig. 6 **a** UV-vis spectra of the Cu₂O-TiO₂ NTAs and absorption get expanded to visible light range and raised with the loading amount of Cu₂O. **b** Visible-light photocatalytic degradation kinetics of MO treated by the heterojunction films with different Cu₂O content. When decoration magnitude of Cu₂O on TiO₂ NTAs increased, the MO decomposition efficiency under visible light irradiation raised. Sample S0 referred to pure TiO₂ film, and sample S1–S5 were the samples immersed in Cu(Ac)₂ solution with the concentrations of 0.05, 0.1, 0.2, 0.3, and 4 mol/L, respectively

decorating Cu₂O nanoparticles. UV-vis along with SEM, EDS, and XRD results proved that the Cu₂O-TiO₂ NTA heterojunction was fabricated successfully by the thermal decomposition method, and samples showed the enhanced visible light absorption.

Photocatalytic activities, one of the most important properties of the Cu₂O-TiO₂ NTA films, were evaluated through degradation of MO aqueous solution. The visible-light photocatalytic degradation kinetics was shown in Fig. 6b. The MO degradation rate was proportion to the loading amount of Cu₂O approximately. The more Cu₂O particles were loaded on TiO₂ NTAs, the faster MO got degraded. Sample S1 degraded MO to 91.0% in 3 h under visible light irradiation, while sample S4 degraded MO to 86.4% in 3 h under the same condition. MO degradation rate represented the photocatalytic activity of the samples. Comparing with the photocatalytic degradation rate to the ~2.73% of CdTe-TiO₂ by a pulse electrodeposited method [29], ~45% of Bi₂O₃ by a ultrasonication-assisted successive ionic layer adsorption and reaction (SILAR) technique [32], and ~27.25%

of Cu₂O by a square wave voltammetry method [33], photoactivity of this as-synthesized Cu₂O-TiO₂ sample was improvable. However, as a facile new strategy, it still conducted to improve fabrication method. When the Cu₂O loading amount went up, there was a trend that the photocatalytic activity of our as-synthesized Cu₂O-TiO₂ NTA heterojunction films increased. It indicated the Cu₂O content had a positive influence of the visible-light photocatalytic activity. TiO₂ itself only responded to ultraviolet, and the visible light range photocatalytic ability should come from the decoration of Cu₂O. As shown in Fig. 7, the conduction band bottom of Cu₂O was a little higher than that of TiO₂, while the valence band top of Cu₂O was higher than that of TiO₂. So, the photoinduced electrons were excited to the conduction band of Cu₂O and then transferred to the conduction band of TiO₂. As a direct-gap semiconductor, wave vector of Cu₂O was just the same at the bottom of the conduction band and the top of valence band. It meant that only the changes of energy were required, instead of the changes of momentum. This

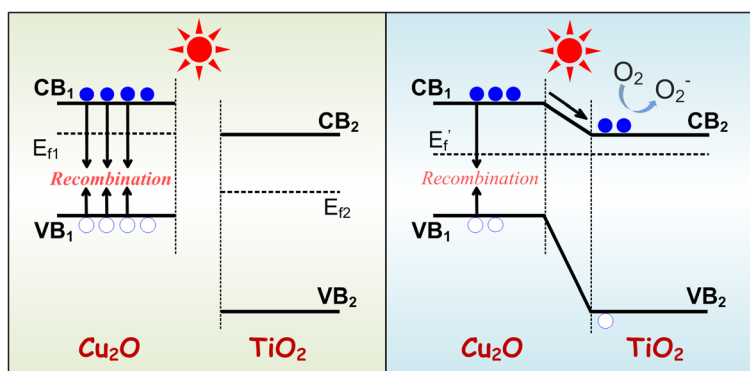


Fig. 7 Band gap structure of Cu₂O and TiO₂ before (left) and after (right) contact. When the Cu₂O-TiO₂ heterojunction is formed, the electron/hole pairs photogenerated on Cu₂O could transfer to TiO₂ NTAs

energy band structure led to the situation that carriers recombined easily. However, due to the help of heterojunction structure, the photogenerated electrons on Cu₂O transferred to TiO₂ NTAs which suppressed the recombination of electron/hole pairs. The longer the pairs existed, the more easily the ROS got produced which brought this photocatalytic activity. As more Cu₂O loaded on TiO₂ NTAs, the heterojunction fabricated better. And the photocatalytic ability got promoted. So, the Cu₂O content showed a positive influence of the visible-light photocatalytic activity. However, further increase of Cu₂O content as well as the photocatalytic ability is limited, due to the solubility of Cu(Ac)₂ in aqueous solution which was 7.2 g (0.36 mol/L) at room temperature. And sample S5 with Cu(Ac)₂ concentration of 4.0 mol/L is prepared by a cycling immerse process described in Additional file 1, the Experimental Details part. The photocatalytic degradation of the MO followed pseudo-first-order kinetics [42] and the kinetic reaction could be expressed as:

$$A_t = A_0 e^{-kt} \quad (4)$$

While our degradation curve showed nearly a straight line, it is not an exponential function. So, there was still room for improvement. And the solubility limit could be broken by the repeated immersion method we mentioned before, with further investigation of the Cu(Ac)₂ concentration and repetition times to avoid adverse effects. In this study, as this thermal decomposition method was what we concerned and tried to illustrate, we just took the 0.3 mol/L (close the solubility of 0.36 mol/L) as the maximum concentration of Cu(Ac)₂ solution. And the photocatalytic activity in visible light range of our as-synthesized heterojunction was confirmed by the MO degradation results. Our previous study found that the Degussa P25 had similar ultraviolet photocatalytic activities with TiO₂ NTAs, when the power P25 was placed on a glass substrate [28]. It can be concluded that we have successfully prepared Cu₂O-TiO₂ NTA heterojunction films with visible-light photocatalytic activities.

Conclusions

In summary, we have successfully prepared the Cu₂O-TiO₂ NTA heterojunction films by a simple thermal decomposition process. SEM, EDS, and XRD results show that TiO₂ NTAs with a tube diameter of ~100 nm were loaded by Cu₂O nanoparticles with an average size of ~50 nm. The anodic TiO₂ NTAs functioned as both “nano-container” and “nano-reactors” to load and synthesize the narrow-band Cu₂O nanoparticles, which has not reported before. UV-vis spectra indicate that the

absorption range of the TiO₂ NTAs was expanded from ultraviolet range to visible light range, due to the loading of Cu₂O. Photocatalytic testing indicated that there was a visible-light photocatalytic activity of the as-synthesized Cu₂O-TiO₂ heterojunction. The photocatalytic abilities of the Cu₂O-TiO₂ NTA heterojunction films were found to be increased with the Cu₂O content from 0.05 to 0.3 mol/L. Our current work has demonstrated a novel and facile method to prepare Cu₂O-TiO₂ NTA heterojunction films, which could also be promising for environmental and energy-related areas.

Additional file

Additional file 1: The experimental details of preparing the Cu₂O-TiO₂ samples and further characterization results of Raman spectra and XRD patterns are provided as the supplemental information to support the discussion. (DOCX 2387 kb)

Abbreviations

EDS: Energy-dispersive spectrometry; NTAs: Nanotube arrays; SEM: Scanning electron microscopy; XRD: X-ray diffraction

Funding

This work was financially supported by the National R&D Program of China under Nos.2017YFA0207400 and 2016YFA0300801, National Natural Science Foundation of China under Nos.51502033, 61734002, and 61571079, and Fundamental Research Funds for the Central Universities of China, No.2672018ZYGX2018J030.

Availability of Data and Materials

They are all in the main text and figures.

Authors' Contributions

YL conceived and supervised the research. PD and XW conducted the experiments and wrote the manuscript. DZ, FL, QY, and HZ made the theoretical analysis. ZZ checked this article and put forward some revised opinions. All the authors discussed the results. All authors read and approved the final manuscript.

Competing Interests

The authors declare that they have no competing interests.

Publisher's Note

Springer Nature remains neutral with regard to jurisdictional claims in published maps and institutional affiliations.

Received: 11 June 2018 Accepted: 13 July 2018

Published online: 24 July 2018

References

1. Qu X, Brame J, Li Q, Alvarez PJJ (2013) Nanotechnology for a safe and sustainable water supply: enabling integrated water treatment and reuse. *Acc Chem Res* 46:834–843
2. Lim YW, Tang Y, Cheng YH, Chen Z (2010) Morphology, crystal structure and adsorption performance of hydrothermally synthesized titania and titanate nanostructures. *Nanoscale* 2:2751–2757
3. Choudhury B, Borah B, Choudhury A (2012) Extending photocatalytic activity of TiO₂ nanoparticles to visible region of illumination by doping of cerium. *Photochem Photobiol* 88:257–264
4. Dholam R, Patel N, Adami M, Miotello A (2009) Hydrogen production by photocatalytic water-splitting using Cr- or Fe-doped TiO₂ composite thin films photocatalyst. *Int J Hydrog Energy* 34:5337–5346
5. Brame JA, Hong SW, Lee J, Lee SH, Alvarez PJ (2013) Photocatalytic pre-treatment with food-grade TiO₂ increases the bioavailability and bioremediation potential of

- weathered oil from the Deepwater Horizon oil spill in the Gulf of Mexico. *Chemosphere* 90:2315–2319
6. Jiang Z, Tang Y, Tay Q, Zhang Y, Malyi OI, Wang D, Deng J, Lai Y, Zhou H, Chen X, Dong Z, Chen Z (2013) Understanding the role of nanostructures for efficient hydrogen generation on immobilized photocatalysts. *Adv Energy Mater* 3:1368–1380
 7. Fischer BB, Krieger-Liszka A, Eggen RIL (2004) Photosensitizers neutral red (type I) and rose bengal (type II) cause light-dependent toxicity in *Chlamydomonas reinhardtii* and induce the Gpx gene via increased singlet oxygen formation. *Environ Sci Technol* 38:6307–6313
 8. Thelese Ru Bao F, Chan KL, Hu X (2012) Structure and properties of nano-confined poly(3-hexylthiophene) in nano-array/polymer hybrid ordered-bulk heterojunction solar cells. *Nanoscale* 4:478–485
 9. Foong TRB, Shen Y, Hu X, Sellinger A (2010) Template-directed liquid ALD growth of TiO₂ nanotube arrays: properties and potential in photovoltaic devices. *Adv Funct Mater* 20:1390–1396
 10. Jha PK, Gupta SK, Lukacevic I (2013) Electronic structure, photocatalytic properties and phonon dispersions of X-doped (X = N, B and Pt) rutile TiO₂ from density functional theory. *Solid State Sci* 22:8–15
 11. Mankad V, Gupta SK, Jha PK (2011) Low frequency Raman scattering of anatase titanium dioxide nanocrystals. *Physica E-Low-Dimensional Syst Nanostruct* 44:614–617
 12. Mohapatra SK, Misra M, Mahajan VK, Raja KS (2007) Design of a highly efficient photoelectrolytic cell for hydrogen generation by water splitting: application of TiO_{2-x}C_x nanotubes as a photoanode and Pt/TiO₂ nanotubes as a cathode. *J Phys Chem C* 111:8677–8685
 13. Gong D, Grimes CA, Varghese OK, Hu WC, Singh RS, Chen Z, Dickey EC (2001) Titanium oxide nanotube arrays prepared by anodic oxidation. *J Mater Res* 16:3331–3334
 14. Grimes CA (2007) Synthesis and application of highly ordered arrays of TiO₂ nanotubes. *J Mater Chem* 17:1451–1457
 15. Lai Y, Gao X, Zhuang H, Huang J, Lin C, Jiang L (2009) Designing superhydrophobic porous nanostructures with tunable water adhesion. *Adv Mater* 21:3799–3803
 16. Macak JM, Schmuki P (2006) Anodic growth of self-organized anodic TiO₂ nanotubes in viscous electrolytes. *Electrochim Acta* 52:1258–1264
 17. Roy P, Berger S, Schmuki P (2011) TiO₂ nanotubes: synthesis and applications. *Angewandte Chemie-Int Ed* 50:2904–2939
 18. Khan MA, Akhtar MS, Woo SI, Yang OB (2008) Enhanced photoresponse under visible light in Pt ionized TiO₂ nanotube for the photocatalytic splitting of water. *Catal Commun* 10:1–5
 19. Macak JM, Zlamal M, Krysia J, Schmuki P (2007) Self-organized TiO₂ nanotube layers as highly efficient photocatalysts. *Small* 3:300–304
 20. Mishra S, Jha PK, Pratap A (2012) Study of size-dependent glass transition and Kauzmann temperature of titanium dioxide nanoparticles. *J Therm Anal Calorim* 107:65–68
 21. Wang P, Tang Y, Dong Z, Chen Z, Lim T-T (2013b) Ag-AgBr/TiO₂/RGO nanocomposite for visible-light photocatalytic degradation of penicillin G. *J Mater Chem A* 1:4718–4727
 22. Wang S, Qian H, Hu Y, Dai W, Zhong Y, Chen J, Hu X (2013a) Facile one-pot synthesis of uniform TiO₂-Ag hybrid hollow spheres with enhanced photocatalytic activity. *Dalton Trans* 42:1122–1128
 23. Xiu Z-m, Zhang Q-b, Puppala HL, Colvin VL, Alvarez PJJ (2012) Negligible particle-specific antibacterial activity of silver nanoparticles. *Nano Lett* 12:4271–4275
 24. Choudhury B, Choudhury A (2013) Oxygen vacancy and dopant concentration dependent magnetic properties of Mn doped TiO₂ nanoparticle. *Curr Appl Phys* 13:1025–1031
 25. Park JH, Kim S, Bard AJ (2006) Novel carbon-doped TiO₂ nanotube arrays with high aspect ratios for efficient solar water splitting. *Nano Lett* 6:24–28
 26. Woan K, Pyrgiotakis G, Sigmund W (2009) Photocatalytic carbon-nanotube-TiO₂ composites. *Adv Mater* 21:2233–2239
 27. Zheng Q, Zhou B, Bai J, Li L, Jin Z, Zhang J, Li J, Liu Y, Cai W, Zhu X (2008) Self-organized TiO₂ nanotube array sensor for the determination of chemical oxygen demand. *Adv Mater* 20:1044–1049
 28. Liao Y, Brame J, Que W, Xiu Z, Xie H, Li Q, Fabian M, Alvarez PJ (2013a) Photocatalytic generation of multiple ROS types using low-temperature crystallized anodic TiO₂ nanotube arrays. *J Hazard Mater* 260:434–441
 29. Feng H, Tran TT, Chen L, Yuan L, Cai Q (2013) Visible light-induced efficiently oxidative decomposition of p-nitrophenol by CdTe/TiO₂ nanotube arrays. *Chem Eng J* 215:591–599
 30. Yang H, Fan W, Vaneski A, Susha AS, Teoh WY, Rogach AL (2012) Heterojunction engineering of CdTe and CdSe quantum dots on TiO₂ nanotube arrays: intricate effects of size-dependency and interfacial contact on photoconversion efficiencies. *Adv Funct Mater* 22:2821–2829
 31. Cai F, Yang F, Zhang Y, Ke C, Cheng C, Zhao Y, Yan G (2014) PbS sensitized TiO₂ nanotube arrays with different sizes and filling degrees for enhancing photoelectrochemical properties. *Phys Chem Chem Phys* 16:23967–23974
 32. Ge M, Cao C, Li S, Zhang S, Deng S, Huang J, Li Q, Zhang K, Al-Deyab SS, Lai Y (2015) Enhanced photocatalytic performances of n-TiO₂ nanotubes by uniform creation of p-n heterojunctions with p-Bi₂O₃ quantum dots. *Nanoscale* 7:11552–11560
 33. Zhang J, Wang Y, Yu C, Shu X, Jiang L, Cui J, Chen Z, Xie T, Wu Y (2014) Enhanced visible-light photoelectrochemical behaviour of heterojunction composite with Cu₂O nanoparticles-decorated TiO₂ nanotube arrays. *New J Chem* 38:4975–4984
 34. Mazare A, Liu N, Lee K, Killian MS, Schmuki P (2013) Embedded palladium activation as a facile method for TiO₂-nanotube nanoparticle decoration: Cu₂O-induced visible-light photoactivity. *Chemistryopen* 2:21–24
 35. Li H, Lai Y, Huang J, Tang Y, Yang L, Chen Z, Zhang K, Wang X, Tan LP (2015) Multifunctional wettability patterns prepared by laser processing on superhydrophobic TiO₂ nanostructured surfaces. *J Mater Chem B* 3:342–347
 36. Seong WM, Kim DH, Park IJ, Do Park G, Kang K, Lee S, Hong KS (2015) Roughness of Ti substrates for control of the preferred orientation of TiO₂ nanotube arrays as a new orientation factor. *J Phys Chem C* 119:13297–13305
 37. Zhong P, Que W, Liao Y, Zhang J, Hu X (2012) Improved performance in dye-sensitized solar cells by rationally tailoring anodic TiO₂ nanotube length. *J Alloys Compd* 540:159–164
 38. Liao YL, Zhang HW, Que WX, Zhong P, Bai FM, Zhong ZY, Wen QY, Chen WH (2013b) Activating the single-crystal TiO₂ nanoparticle film with exposed {001} facets. *ACS Appl Mater Interfaces* 5:6463–6466
 39. Hanaor DAH, Sorrell CC (2011) Review of the anatase to rutile phase transformation. *J Mater Sci* 46:855–874
 40. Kandiel TA, Robben L, Alkaim A, Bahnemann D (2013) Brookite versus anatase TiO₂ photocatalysts: phase transformations and photocatalytic activities. *Photochem Photobiol Sci* 12:602–609
 41. Brandt IS, Martins CA, Zoldan VC, Viegas ADC, da Silva JHD, Pasa AA (2014) Structural and optical properties of Cu₂O crystalline electrodeposited films. *Thin Solid Films* 562:144–151
 42. Liao Y, Zhang H, Zhong Z, Jia L, Bai F, Li J, Zhong P, Chen H, Zhang J (2013c) Enhanced visible-photocatalytic activity of anodic TiO₂ nanotubes film via decoration with CuInSe₂ nanocrystals. *ACS Appl Mater Interfaces* 5:11022–11028

Submit your manuscript to a SpringerOpen[®] journal and benefit from:

- Convenient online submission
- Rigorous peer review
- Open access: articles freely available online
- High visibility within the field
- Retaining the copyright to your article

Submit your next manuscript at ► springeropen.com